Available online at www.sciencedirect.com
SCIENCE DIRECT®
Physica D 206 (2005) 145–165
PHYSICA D
www.elsevier.com/locate/physd

A numerical study of one-step models of polymerization: Frontal versus bulk mode

Stephen A. Cardarelli[1], Dmitry Golovaty*,[2], L.K. Gross, Vitaliy T. Gyrya, Jianping Zhu

Department of Theoretical and Applied Mathematics, The University of Akron, Akron, OH 44325, USA

Received 8 April 2004; received in revised form 5 August 2004; accepted 10 January 2005
Available online 4 June 2005
Communicated by C.K.R.T. Jones

Abstract

In free-radical polymerization, a monomer-initiator mixture is converted into a polymer. Depending on initial and boundary conditions, free-radical polymerization can occur either in a bulk mode (BP) or in a frontal mode (FP) via a propagating self-sustaining reaction front. The main goal of this paper is to study the role that bulk polymerization plays in frontal polymerization processes for various one-step kinetics models.

We use numerical simulations to study the influence of reaction kinetics on one-dimensional frontal polymerization. We show that the long-time behavior of systems modeled with discontinuous distributed kinetics (e.g. step-function kinetics) significantly departs from the long-time behavior of systems modeled with Arrhenius kinetics. The difference is due to slow BP in the initial mixture of reagents, which influences both the speed and the long-time stability of the reaction front.

Further, we show that for distributed kinetics a "true" FP is only possible for a steadily propagating, traveling-wave reaction front. When a front propagates in a pulsating mode, we demonstrate the existence of pockets of unreacted monomer behind the front. These pockets evolve via a bulk polymerization mechanism.

A mathematical model of one-step free-radical frontal polymerization is identical to the model of gasless combustion, so bulk reactions play a role in the latter context, as well. However, fronts propagate much faster in combustion than in polymerization, and slow bulk reactions in regions ahead of the burning front can generally be neglected.

PACS: 82.35.−x; 81.20.Ka; 02.30.Oz; 02.70.Bf

Keywords: Frontal polymerization; Gasless combustion; Arrhenius kinetics; Traveling wave

* Corresponding author. Tel.: +1 330 972 8012; fax: +1 330 374 8630.
[1] Supported in part by the NSF grant EHR-0082979.
[2] Supported in part by the NSF grant DMS-0305577.
E-mail addresses: stephen@amrl.uakron.edu (S.A. Cardarelli); dmitry@math.uakron.edu (D. Golovaty); gross@math.uakron.edu (L.K. Gross); vitaliy@amrl.uakron.edu (V.T. Gyrya); jzhu@math.uakron.edu (J. Zhu).
0167-2789/$ – see front matter © 2005 Elsevier B.V. All rights reserved.
doi:10.1016/j.physd.2005.05.005

1. Introduction

1.1. Physical background

We study the interplay between two different modes of free-radical polymerization—frontal polymerization (FP) via a propagating, localized reaction zone [1,2] and bulk polymerization (BP) within a distributed reaction zone. While BP has been widely used in manufacturing of plastics, FP remains at the experimental stage. FP has an advantage over BP in the speed of conversion and has a number of potential uses such as filling or sealing of structural cavities, rapid curing of polymers, and uniform curing of thick polymers [3].

Free-radical polymerization is the process of converting a monomer-initiator mixture into a polymer, which occurs when a thermally unstable initiator is mixed with a monomer. The initiator molecules decompose into radicals that combine with the monomer to form reactive polymer chains (polymer radicals) that continue to grow by incorporating additional molecules of the monomer. The growth may terminate through a reaction with either another reactive polymer chain or an initiator radical. The polymer molecule becomes inactive following the termination step.

The polymerization reactions are exothermic and are modeled with temperature-dependent (Arrhenius) kinetics. In the bulk mode, the temperature of the test tube is raised uniformly throughout the tube, accelerating the polymerization reactions that occur everywhere inside the tube at the same time. In the frontal mode, the reactions are initiated locally and then propagate through the tube via the thin, self-sustaining reaction zone determined by the coupling between the thermal diffusion and the reaction kinetics.

A typical FP experiment can be performed in a glass tube filled with reagents. An external heat source, when applied at the top of the tube, initiates a descending front that appears as a moving region of polymer formation. Depending on the choice of reactants and the conditions of the experiment, the front either may or may not propagate with a constant speed. Various nonuniform propagation scenarios can occur, even if the front always remains flat—the situation considered in this paper.

Several conditions are necessary for the existence of the frontal mode. First, the ignition temperature must be high enough to generate and initially sustain the reaction front. Further, the reaction rate must be extremely small at the initial (ambient) temperature but very large at the front temperature. The high reaction rate coupled with the exothermicity of the reaction must be sufficient to overcome heat losses into the reactants and product zones.

The mode of conversion may also depend on the physical state of both reagents and the final product. In particular, the monomer can be a liquid and the polymer can be either a solid or a very viscous liquid [3]. To minimize flow transport in the system, the viscosity of the monomer can be increased by adding to the system inactive components such as silica gel [3]. Here we will assume that both reagents and the final product are viscous enough for us not to be concerned with convective effects and bubble formation that affect the polymerization dynamics in the liquid phase.

A more extensively studied chemical process with a similar reaction mechanism is self-propagating high-temperature synthesis (SHS)—a combustion process characterized by a heat release large enough to propagate a combustion front through a powder compact, while consuming the reactant powders [4,5]. The simplest models and front propagation mechanisms for FP and SHS are essentially the same, except for the magnitudes of the model parameters. These differences in parameter values may lead to the differences in observable long-time behavior between systems undergoing SHS and FP, as will be discussed later in this paper.

Several different zones are usually distinguished in materials undergoing SHS: reactants zone, heating zone where chemical reactions have not yet been initiated, a reaction zone, and a final product zone that has no influence on the velocity of the combustion wave. A similar zone structure characterizes mixtures undergoing frontal polymerization.

Both steady and unsteady combustion wave propagation have been observed in SHS. The wave velocity in SHS is of order 10^{-3} to 10^{-2} m/s [6,7]. Note for comparison that the front velocity in FP is of order 10^{-4} m/s [8].

Unsteady wave propagation was first predicted for SHS in a one-dimensional model where the combustion wave was found to propagate with an oscillating speed [9,6]. The rise of this instability is usually explained

through the following series of observations that pertain to both SHS and FP.

During steady propagation of the reaction wave, a balance is maintained between the heat released during the reaction and the heat diffused into the mixture of reagents. However, when the activation energy of the reaction is sufficiently high, this balance may become upset.

Once a front of a highly exothermic reaction is initiated, a significant amount of heat is released and the temperature of the reaction zone exceeds the adiabatic temperature. The excess heat diffuses rapidly toward the reactants, lowering the temperature of the reaction zone and slowing down both the conversion process and the velocity of the front. Subsequently, the heat exchange between the reaction zone and the heating zone "preheats" the reagents, eventually leading to a "splash"—a high-temperature reaction wave propagating over a preheated reactive mixture. Gradually, the reaction front enters the region containing a cooler mixture and the temperature of the reaction zone decreases, suppressing the rate of the front propagation. The heat exchange between the reaction zone and the heating zone becomes dominant again and the process repeats itself.

Unsteady front propagation is usually undesirable in manufacturing. One of the goals of the modeling is to determine the range of material parameters within which the stability of the uniformly propagating polymerization front is guaranteed. In order for the parameter ranges to be valid, a correct modeling procedure must be followed. If the full model is too complicated to analyze, its approximations may be considered instead; however, their validity must also be addressed. For the simplest SHS and FP problems, the simplifications usually reduce to choosing an appropriate approximation of the Arrhenius kinetics function motivated by the presence of a small parameter.

In this paper, we use numerical simulations to study the influence of reaction kinetics on one-step frontal polymerization in one dimension. We show that the long-time behavior of systems governed by approximate kinetics (sharp-front, step-function) significantly differs from the long-time behavior of systems governed by Arrhenius kinetics. The differences are caused by slow bulk reactions in the initial mixture of reagents that influence both the speed and the long-time stability of the reaction front. Although these reactions can be neglected in combustion problems because of very high speeds of front propagation, they may play a role in FP, where these speeds are much slower.

Further, we show that for distributed kinetics a "true" FP is only possible for a steadily propagating, traveling wave reaction front. When a front propagates in a pulsating mode, we demonstrate the existence of pockets of unreacted monomer behind the front. These pockets evolve via the bulk polymerization mechanism.

1.2. Mathematical models

Although the mechanism of free-radical polymerization involves three steps—initiation, propagation, and termination—and five reagents—an initiator, an active initiator radical, an active polymer radical, a monomer, and a complete polymer chain [10], a number of simplifying assumptions can be made that reduce the complexity of the underlying mathematical model. Hence, we will assume [10–12] that

- The rates of reactions between the initiator radicals and the monomer and between the polymer radicals and the monomer are the same.
- The rate of change of total radical concentration is much smaller than the rates of their production and consumption.
- The initial concentration of the initiator is so large that it is not appreciably consumed during the polymerization process.
- The material diffusion is negligible compared to thermal diffusion.

Suppose that a test tube containing the monomer-initiator mixture occupies a region $\Omega \in \mathbf{R}^3$, and denote by $M(x,t)$ the monomer concentration and by $T(x,t)$ the temperature of the mixture at the point $x \in \Omega$ and the time $t > 0$. Then the process of free-radical polymerizations can be described [12] by what is known as a single-step, effective kinetics model of monomer-to-polymer conversion

$$\frac{\partial M}{\partial t} = -kM\mathrm{e}^{E/R_\mathrm{g}T_\mathrm{b}(1-(T_\mathrm{b}/T))}, \tag{1}$$

$$\frac{\partial T}{\partial t} = \operatorname{div}(\kappa\nabla T) + kqM\mathrm{e}^{E/R_\mathrm{g}T_\mathrm{b}(1-(T_\mathrm{b}/T))}, \tag{2}$$

where κ is the thermal diffusivity of the mixture/final product, k is the effective pre-exponential factor in the Arrhenius kinetics, R_g is the gas constant, E is the effective activation energy, and T_b is a reference temperature that will be specified below. The constant parameter q is $\Delta H/c\rho$, where ΔH is the reaction enthalpy; c and ρ are the specific heat and the mixture density, respectively.

Throughout this paper we will assume that the test tube is one-dimensional, $\Omega = [-L, L]$, and that the thermal diffusivity κ is constant (ignoring possible dependence of κ on temperature and degree of conversion $1 - M/M_0$). Then the problem (1) and (2) reduces to

$$\frac{\partial M}{\partial t} = -kM e^{E/R_g T_b(1-(T_b/T))}, \tag{3}$$

$$\frac{\partial T}{\partial t} = \kappa \frac{\partial^2 T}{\partial x^2} + kqM e^{E/R_g T_b(1-(T_b/T))}. \tag{4}$$

We will assume that T and M satisfy the constant initial conditions

$$T(x,0) = T_0,\ M(x,0) = M_0,\ x \in [-L, L]. \tag{5}$$

In order to initiate the reaction, heat must be supplied to the system; hence for the first t_0 seconds we will use the following boundary conditions

$$T_x(-L,t) = 0,\ M_x(\pm L,t) = 0,\ T(L,t) = T_b,\ t \in (0,t_0). \tag{6}$$

During the front propagation regime, we will impose the adiabatic and impenetrability boundary conditions on the temperature and the monomer concentration, respectively by setting

$$T_x(\pm L,t) = 0,\ M_x(\pm L,t) = 0,\ t \geq t_0. \tag{7}$$

Multiplying (3) by q, adding the resulting equation to (4), integrating with respect to x, applying the adiabatic boundary conditions in (7), and setting

$$H := \int_{-L}^{L} (T + qM)\,\mathrm{d}x \tag{8}$$

yield

$$\frac{\mathrm{d}H}{\mathrm{d}t} = 0 \tag{9}$$

when $t > t_0$, expressing conservation of enthalpy in the system. Thermodynamics of the problem dictates that the temperature of the reaction products away from the front is given by

$$T_b = T_0 + qM_0, \tag{10}$$

where T_0 and M_0 are the initial temperature and concentration, respectively, in (5).

We introduce dimensionless parameters

$$\epsilon = \frac{R_g T_b}{E},\ Z = \frac{qM_0 E}{R_g T_b^2}, \tag{11}$$

and dimensionless variables

$$\tilde{t} = \frac{kt}{Z},\ \tilde{x} = \sqrt{\frac{k}{Z\kappa}}x,\ \tilde{M} = \frac{M}{M_0},\ \tilde{T} = \frac{T - T_0}{T_b - T_0}.$$

Here T_b is as defined in (10) and the Zeldovich number Z is a non-dimensionalized activation energy [13] constructed as a ratio of the diffusion temperature scale $T_b - T_0$ to the reaction temperature scale $R_g T_b^2/E$. Also, note that $Z\epsilon < 1$ in order to ensure that the initial temperature of the mixture is greater than absolute zero. Then (after dropping tildes) we obtain

$$\frac{\partial M}{\partial t} = -ZM \exp\left(\frac{Z(T-1)}{\epsilon Z(T-1)+1}\right), \tag{12}$$

$$\frac{\partial T}{\partial t} = \frac{\partial^2 T}{\partial x^2} + ZM \exp\left(\frac{Z(T-1)}{\epsilon Z(T-1)+1}\right). \tag{13}$$

Non-dimensionalizing the conditions (5)–(7) yields

$$T(x,0) = 0,\ M(x,0) = 1,\ x \in [-l, l], \tag{14}$$

$$M_x(\pm l,t) = 0,\ T_x(-l,t) = 0,\ T(l,t) = 1,\ t \in (0,\tau_0), \tag{15}$$

$$M_x(\pm l,t) = 0,\ T_x(\pm l,t) = 0,\ t \geq \tau_0, \tag{16}$$

where $l = \sqrt{k/Z\kappa}L$ and $\tau_0 = k\,t_0/Z$.

Eqs. (12) and (13) are not amenable to an analytical approach. Various approximations to the kinetics simplify the problem.

Conversion occurs primarily in a thin reaction zone, slowly ahead of the zone, and not at all behind the zone. A point-source approximation in both FP and SHS exploits the narrowness of the reaction zone.

The δ-function sharp-front approximation of the reaction propagation in solid fuel combustion was studied in [14] in the case when $\epsilon \ll 1$. The sharp-front

approximation and the strength of the heat source term follow from the analysis similar to [15].

In [12], a sharp front approximation is combined with the step function kinetics to describe frontal polymerization. To start, the authors replaced the Arrhenius kinetics with a step function of height equal to the maximum of the Arrhenius function, as in [16]. The step-function kinetics was chosen such that its integral value on $[T_0, T_b]$ approximately equaled the integral value of the Arrhenius kinetics function on the same interval. Generally, T_b and, hence, the step function can be functions of time. In [12], only the sharp-front approximation was considered, under the assumption that the dimensionless parameter ϵ was small.

Here we will consider a diffused version [17] of the step-function kinetics as one of two approximations to compare with the full kinetics of (12) and (13). In addition, we use Arrhenius kinetics with a cutoff, as in the solid combustion context [18].

Approximate kinetics in the literature and in this paper recast the problem such that traveling-wave solutions exist. These lead to bifurcation and stability analyzes.

In gasless combustion, a solution exhibiting a periodically pulsating, propagating reaction front arises as a Hopf bifurcation from a solution describing a uniformly propagating front in [14]. The bifurcation parameter is the Zeldovich number Z, defined in (11). Amplitude, frequency, and velocity of the propagating front were determined in nonlinear analysis. It was also demonstrated analytically that the mean velocity of the pulsating front is less than the velocity of the uniformly propagating front. A similar, δ-function approach was also adopted in [19] to perform a stability analysis.

Linear stability analyses for FP appear in a number of papers, e.g. [12]. For a weakly nonlinear analysis in this context, see [20].

Various works have explored numerically the dynamics of models with approximate kinetics, for both SHS and for FP. For instance, in [21], Arrhenius kinetics with a cutoff was used to observe chaotic pulsations, following a number of period-doubling bifurcations.

A free-interface problem for the point-source model in combustion has been studied numerically in [22]. For a sufficiently large Z, the work showed transitions to chaos via a period-doubling solution and highly irregular relaxational oscillations. Increasing the bifurcation parameter lead to enhanced fluctuations and a reduction of the average velocity of propagation. The authors attributed a lack of sequential secondary bifurcations to the difference between the point-source and distributed-kinetics models (as in [21]). However, the entire spectrum of behavior for distributed kinetics was found later for the point-source model in [23].

The literature also contains numerical studies of the full Arrhenius kinetics. For example, the propagation of a pulsating front of an exothermic reaction in a condensed phase was studied numerically in [24] for the model (1) and (2). The stability of the reaction front was determined to depend on a single non-dimensional parameter

$$\alpha = 9.1\, Z^{-1} - 2.5\epsilon. \tag{17}$$

It was shown that if $\alpha > 1$ then the stationary reaction is stable. If $\alpha < 1$ then the reaction propagates in a pulsating regime. It was specifically noted that the structure of the front oscillations depends on α only and not on Z or ϵ separately. Additional bifurcations were observed as α decreased further away from the threshold of stability; the average velocity of the front propagation was observed to decrease with α.

In [25], period doubling in gasless combustion leading to chaos was demonstrated numerically, depending on the values of activation energy and the heat of reaction. Doubling of up to the period eight was reported with regions of existence of each consecutive solution getting narrower and narrower.

In this paper we compare and contrast the computed dynamics of three models: two with different forms of approximate kinetics and one with the full Arrhenius kinetics. In the first approximation, a cutoff function multiplies the Arrhenius kinetics to eliminate bulk reactions ahead of the advancing front. The cutoff function in terms of dimensional variables is

$$\chi(x\,,t) = \begin{cases} 0, & T(x,t) \le (1+\delta)T_0, \\ 1, & T(x,t) > (1+\delta)T_0. \end{cases} \tag{18}$$

Here $\delta = 10^{-4}$, which is small enough to ensure that the reaction is switched off well ahead of the front.

To formulate the step-function-kinetics model [17] we assume that ϵ is small; then the system of Eqs. (12) and (13) reduces to

$$\frac{\partial M}{\partial t} = -ZM\mathrm{e}^{Z(T-1)}, \tag{19}$$

$$\frac{\partial T}{\partial t} = \frac{\partial^2 T}{\partial x^2} + ZM\mathrm{e}^{Z(T-1)}. \tag{20}$$

Next we replace the Arrhenius kinetics $Z\,\mathrm{e}^{Z(T-1)}$ in (19) and (20) by the step-function

$$K(T) := \begin{cases} 0\,, & T < T_\mathrm{p} - \frac{1}{Z}\,, \\ Z\,\mathrm{e}^{Z(T_\mathrm{p}-1)}\,, & T \geq T_\mathrm{p} - \frac{1}{Z}\,, \end{cases} \tag{21}$$

where T_p is the temperature of the mixture immediately upon the completion of the reaction (or, analogously, the temperature at the product end of the reaction zone). Since this temperature is, generally, the highest temperature of the mixture, within this model the reaction is assumed to occur in the temperature range $\left[T_\mathrm{p} - (1/Z), T_\mathrm{p}\right]$. Unless the front is a steadily propagating wave, the maximum temperature inside the test tube and, therefore, the shape of the kinetics function depend on time.

Here, we will assume that $T_\mathrm{p}(t) = T(x_\mathrm{b}(t), t)$, where $x_\mathrm{b}(t)$ is a point at which the monomer concentration falls below a prescribed threshold value $M(x_\mathrm{b}(t), t) = \beta$. The appropriate value of the small constant parameter $\beta > 0$ is found to be $\beta = 2.\mathrm{E}{-2}$ by numerical experiment.

2. Numerical simulations

2.1. Numerical method

The governing system of dimensional Eqs. (3) and (4) is solved numerically using a finite difference method with implicit time integration. The nonlinear reaction terms in the equations are linearized using Newton's method. We apply Dirichlet boundary condition $T(L, t) = T_\mathrm{b}$, where T_b is defined in (10), at the ignition end of the domain for a short period of time to initiate the reaction (6), and then switch to the homogeneous Neumann boundary condition (7). Numerical experiments have demonstrated that the long-term behavior of the reaction-diffusion equation system studied in this paper is not affected by the application of the Dirichlet boundary condition during the initiation stage.

At each time step, the reaction front is defined as the first grid point, going from left to right, at which the concentration of the monomer drops below 50% of its value near the endpoint of the domain in the unreacted reagents zone. Note that, mathematically, the value of monomer concentration M is always nonzero. We will choose a threshold monomer concentration m and assume that the polymerization process is finished once the monomer concentration falls below m.

The average velocity of the front is calculated by

$$v = a\frac{\Delta x}{\Delta t}$$

where Δx is the distance between grid points, Δt is the size of the time step, and a is the number of grid intervals traveled through by the front in Δt seconds. Note that it may take multiple, say n, time steps for the front to travel through one grid interval. In that case, we have $a = 1/n$.

Unless specified otherwise, throughout this section we will assume that the parameters

$$q = 33.24\ \mathrm{K^\circ\,L/mol},\ \kappa = 0.0014\,\mathrm{cm^2/s},$$
$$k = 1\,\mathrm{s^{-1}},\ T_\mathrm{b} = 500\,\mathrm{K^\circ},$$

are fixed; then the state of the system is completely determined once the values of Z and ϵ are specified. The length of the spatial domain (test tube) in our computations varies from 4 to 87 cm, depending on the characteristic time scale of the process of interest.

2.2. Code validation: role of boundary conditions

In this section, we validate our code by comparing its predictions with existing numerical results and by demonstrating that the computed solution has the conservation properties predicted by the underlying model.

We begin by showing that our code reproduces the known, numerically determined types of FP and SHS dynamics over a range of Z values for the Arrhenius kinetics (Fig. 1) as have been reported previously by [10,25], and others. The front velocity profiles presented in Fig. 1 were computed using the same data and are in excellent agreement with the results of [10]. In these computations the values of the pre-exponential factor k were adjusted

$$k = 1.07\,\mathrm{s^{-1}} \text{ when } Z = 7.25,$$
$$k = 1.43\,\mathrm{s^{-1}} \text{ when } Z = 8.05,$$

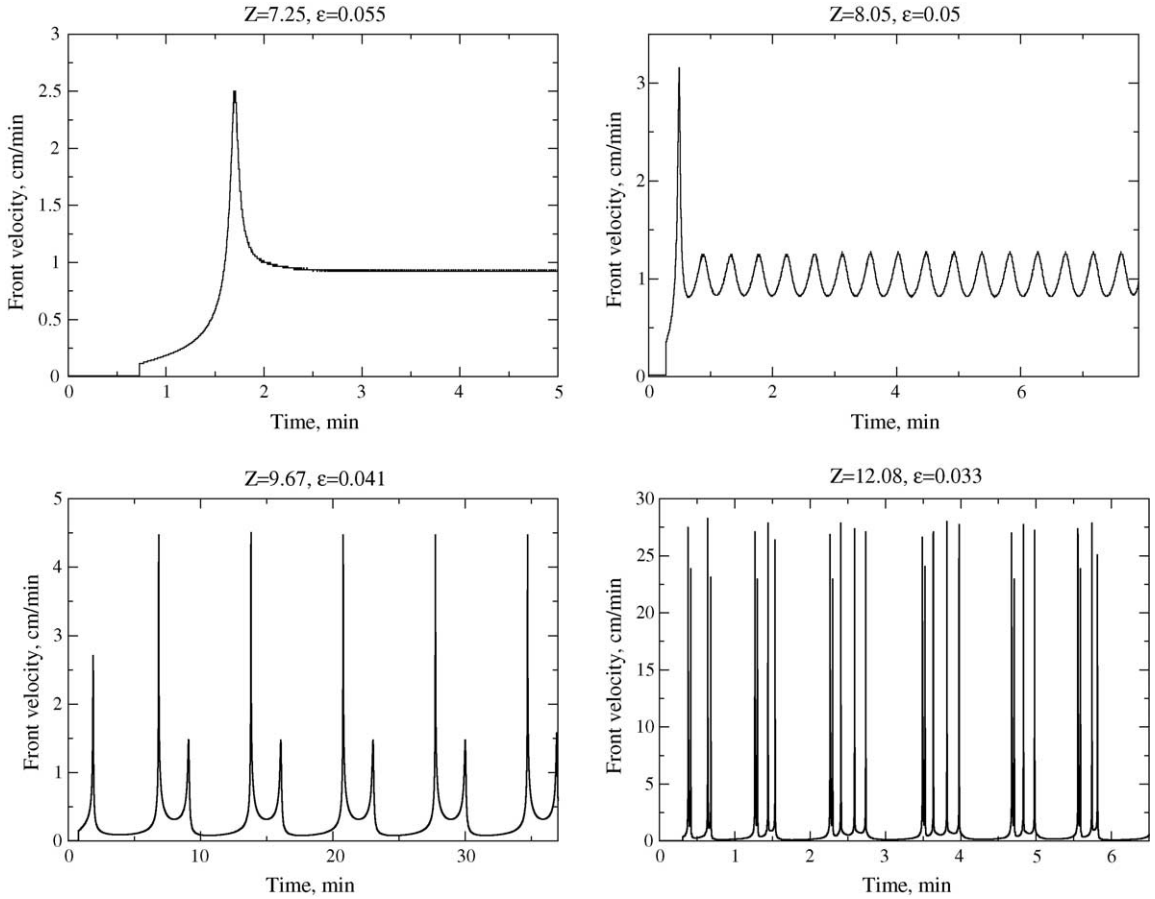

Fig. 1. Possible modes of propagation of the polymerization front.

$k = 0.25\,\mathrm{s}^{-1}$ when $Z = 9.67$,

$k = 6.03\,\mathrm{s}^{-1}$ when $Z = 12.08$.

to match those in [10].

Using the values of ϵ considered in Fig. 1 and (17), the threshold values of Zeldovich number can be found to lie between $Z = 8$ and $Z = 8.41$. Hence, of the four cases, the traveling wave solutions are expected to be stable only when $Z = 7.25$. Indeed, when $Z = 7.25$, following the velocity spike corresponding to the onset of frontal mode, the front settles into propagating at a constant speed. When Z is increased up to $Z = 8.05$, the front propagates in the pulsating mode following the brief transition period. When the Zeldovich number reaches $Z = 9.67$, our results demonstrate period doubling. Chaos begins to develop as the Zeldovich number is increased further.

Fig. 2 shows the results of another test of the validity of our numerical method. To initiate the reaction, we *always* apply the Dirichlet boundary conditions for the first 400 s during the simulations. Following this period, the Dirichlet conditions are either retained for the duration of time or are switched to the adiabatic Neumann conditions once the front begins to advance in the self-propagating mode.

According to (9), the enthalpy H defined in (8) should be preserved under adiabatic conditions on the temperature. The plots of H are shown in Fig.

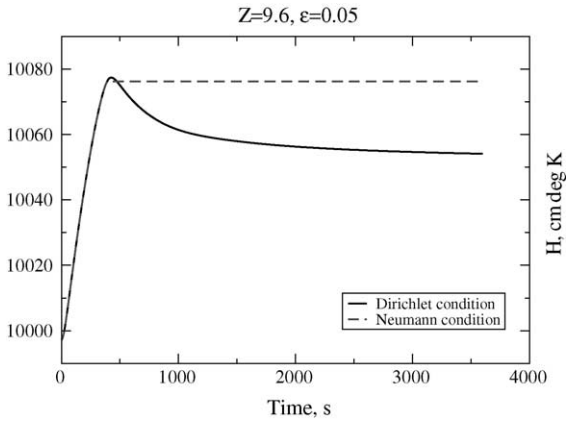

Fig. 2. Enthalpy H vs. time when either the Dirichlet boundary condition on the right side of the tube is applied at all times (solid line) or Dirichlet boundary condition on the right side of the tube is applied for the first 400 s and then switched to a Neumann boundary condition (dashed line).

2 for both Neumann and Dirichlet boundary conditions applied during front-propagating phase when $Z = 9.67$ and $\epsilon = 0.041$. In the former case (dashed line on Fig. 2), the Dirichlet boundary condition was applied for the first 400 s on the reaction (right) side of the test tube. During this period, a substantial amount of heat is supplied into the system as is evident from the rapidly increasing H. On the other hand, once the boundary condition is switched to adiabatic Neumann condition, H becomes independent of time indicating that our numerical method exhibits very little numerical dissipation (dashed line on Fig. 2). When the Dirichlet boundary condition allowing for the heat exchange between the test tube and the environment is maintained for the duration of time, the value of H begins to level off around $t = 1000$ s (solid line on Fig. 2) indicating the essentially adiabatic, self-sustaining nature of the reaction.

Our numerical observations support this conclusion; beyond the transition stage, the front propagation dynamics are essentially indistinguishable for Dirichlet and Neumann boundary conditions (Fig. 3) although, as indicated by Fig. 2, the temperature and monomer distributions themselves are not necessarily the same.

2.3. Arrhenius kinetics versus non-smooth kinetics: long-time stability of polymerization front

Here we investigate the effect of the slow, low-temperature bulk reaction in a mixture of reagents far ahead of the polymerization front on the velocity and asymptotic stability of FP.

For the Arrhenius kinetics, the reaction although very slow still does occur at low temperatures. In solid-state combustion the flame front propagates extremely fast—a front has to advance by distances on the order of thousands of meters—for this bulk reaction to have any appreciable effect [6]. However, in the case of frontal polymerization the propagation speeds are relatively low and the bulk reaction in the initial mixture becomes significant if the long-time behavior of the polymerization front is important. Since the long

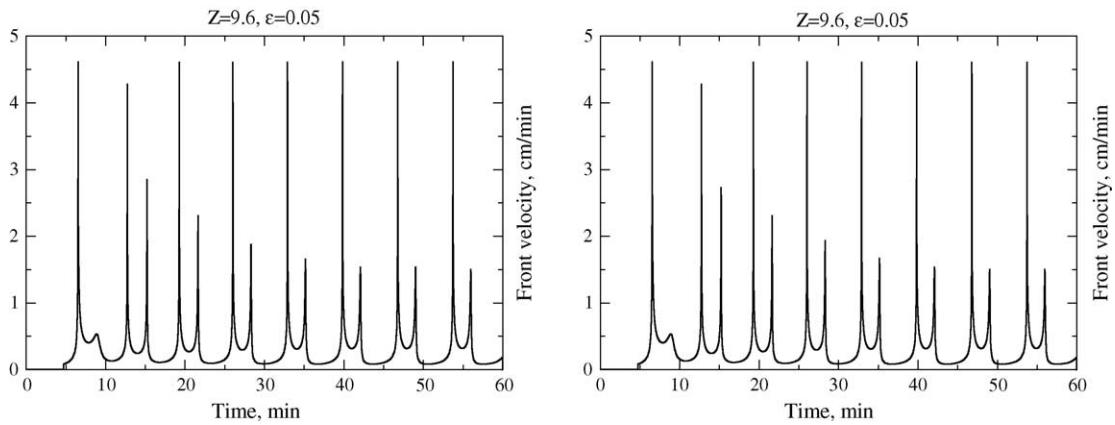

Fig. 3. Front velocity vs. time when either Dirichlet boundary condition on the right side of the tube is applied at all times (left graph) or Dirichlet boundary condition on the right side of the tube is applied for the first 400 s and then switched to a Neumann boundary condition (right graph).

time scale $\bar{t}$ for the low-temperature reaction is on the order of e^{-Z}, one can employ the method of multiple time scales in (12)–(16) to recover the long time scale dependence of the front velocity [20]. This method is identical to quasi-steady analysis of time dependence of the traveling wave velocity in [26].

Since they were developed mostly for combustion-type problems, the majority of popular approximations of the Arrhenius kinetics incorporate some form of cutoff that sets the reaction rate to zero for temperatures below a certain threshold. For example, in [16] the reaction rate is assumed to vanish below the reaction temperature; in [18] the Arrhenius kinetics function is multiplied by a cutoff function to switch off the reaction at distances that exceed a certain critical value ahead of the front to model the fact that the reaction is insignificant in this region. All bulk reactions are clearly neglected within sharp-front approximations (e.g. [14]) as well since all reactions are reduced to a point-source on the interface.

The bulk reaction raises the temperature and lowers the monomer concentration ahead of the advancing polymerization front, thereby having a stabilizing effect on its propagation. Indeed, from the point of view of the stability criterion (17), since the temperature behind the front remains equal to T_b and the non-dimensional Zeldovich number Z is proportional to the monomer concentration in the initial mixture of reagents, the parameter ϵ does not change on the long time scale $\bar{t}$, while the parameter Z decreases with $\bar{t}$, eventually falling below the stability threshold. In order to measure the influence of bulk reaction on the value of the Zeldovich number that is "seen" by the advancing front, we introduce the effective Zeldovich number

$$Z_{\mathrm{eff}}(t) := \frac{qM(a,t)E}{R_g T_b^2} \tag{22}$$

where the point a lies ahead of the front far away from the reaction zone. When the heat diffusion is relatively slow, we expect that Z_{eff} is mainly influenced by bulk reactions.

We compare the results of simulations for the full Arrhenius kinetics, the Arrhenius kinetics multiplied by a cutoff function (18), and step-function kinetics (21).

First, let $Z = 7$. The position and velocity of the polymerization front for the three different types of kinetics are depicted in Figs. 4 and 5, respectively. Observe that, initially, all three kinetics lead to the uniformly propagating polymerization fronts advancing with approximately the same velocities. Although the dynamics of the fronts corresponding to either of the modified kinetics does not change with time, the front corresponding to the Arrhenius kinetics accelerates, and the frontal polymerization is completed by $t \approx 3300$ s (here we assume that m defined in Section 2.1 is equal to 1.E−3, that is the polymerization is considered to be complete once the concentration of the monomer falls below 1.E−3).

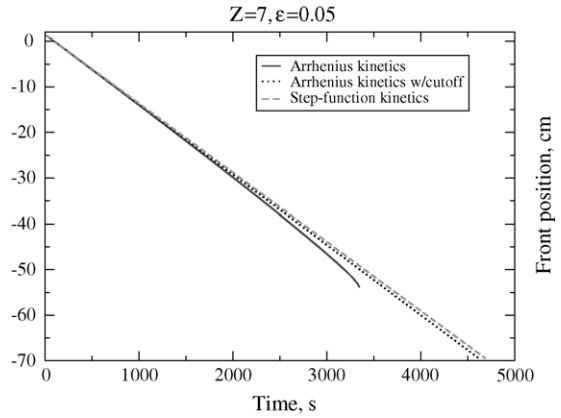

Fig. 4. Position of polymerization front for the various types of kinetics.

The consecutive positions of the reaction front at equally spaced times for both the Arrhenius kinetics and the Arrhenius kinetics with the cutoff are shown in

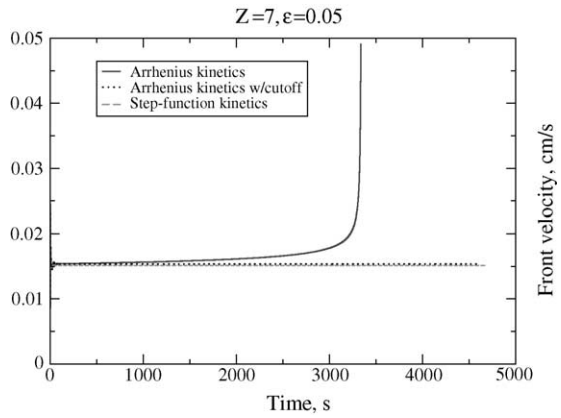

Fig. 5. Velocity of polymerization front for the various types of kinetics.

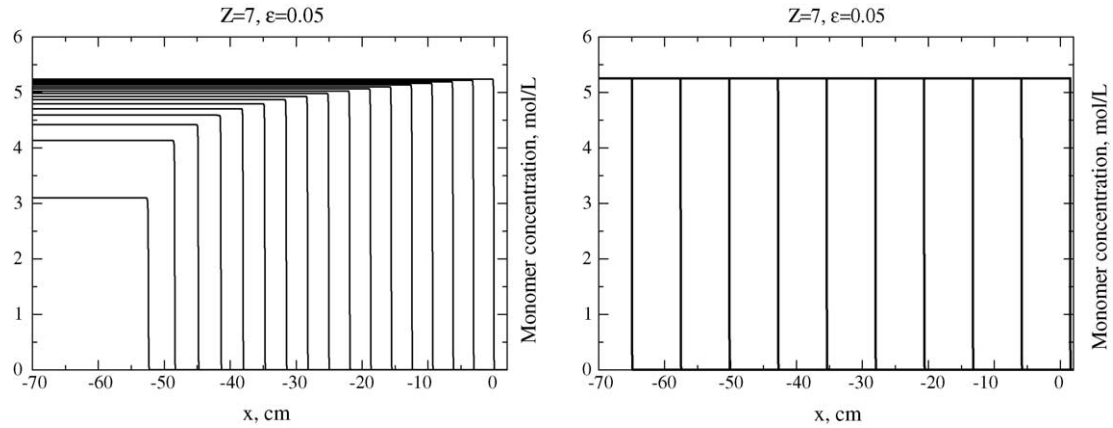

Fig. 6. Snapshots of the monomer profiles at equal time intervals for the Arrhenius kinetics (left) and the Arrhenius kinetics with cutoff (right). The polymerization front propagates to the left.

Fig. 6. Note that, in the system governed by the Arrhenius kinetics with the cutoff, the polymerization front propagates at the same rate and the concentration of the monomer remains constant in the mixture of reagents ahead of the front. On the other hand, the monomer is being depleted in the region ahead of the advancing front in the system governed by the Arrhenius kinetics; the polymerization in this system occurs via both the bulk and the frontal polymerization. The polymerization front exists throughout the polymerization process and propagates at an increasing speed. The effective value of the Zeldovich number shown on Fig. 7 decreases with time for the Arrhenius kinetics and remains unchanged for both the Arrhenius kinetics with a cutoff and step-function kinetics.

Next we consider frontal polymerization systems governed by the Arrhenius kinetics and Arrhenius kinetics with cutoff when $Z = 8.089$ and $\epsilon = 0.05$. According to the stability criterion (17), the uniformly propagating fronts in such systems should be unstable. Indeed, both the front velocity and the front temperature for the Arrhenius kinetics exhibit oscillating profiles as shown in Fig. 8 (cf. Fig. 1). As the front temperature we use the temperature of the mixture when the concentration of the monomer falls below 2% of its initial value; this choice is further elaborated upon in [17]. However, if the simulation is run for significantly longer time, long-time-scale behavior emerges as evidenced by Fig. 9, showing the upper and lower envelopes of the front velocity and the front temperature profiles for both the Arrhenius kinetics and the Arrhenius kinetics with the cutoff. (We use the envelopes for ease of visualization since both quantities are rapidly oscillating on the long time scale.) As the initial condition for these simulations, we used a profile that is "close" to the profile of the uniformly propagating traveling wave corresponding to $Z = 8.089$ and $\epsilon = 0.05$. Clearly this profile is unstable, as demonstrated in Fig. 9 by the initial increase in the amplitude of velocity oscillations (cf. [24]). The front pulsations corresponding to the Arrhenius kinetics with the cutoff then stabilize and retain the same amplitude throughout the simulations; however the amplitude of the front pulsations for the system governed by the Arrhenius kinetics mono-

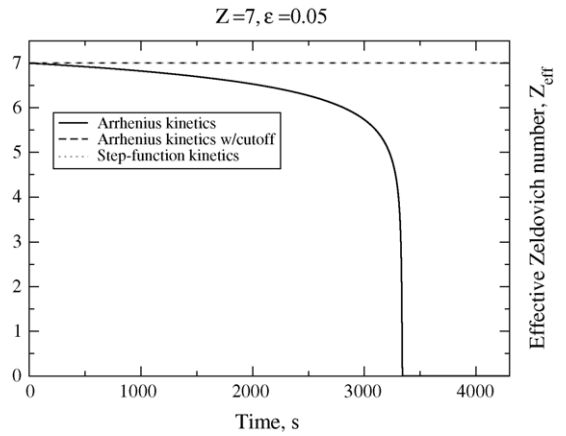

Fig. 7. Effective value of the Zeldovich number for the various types of kinetics.

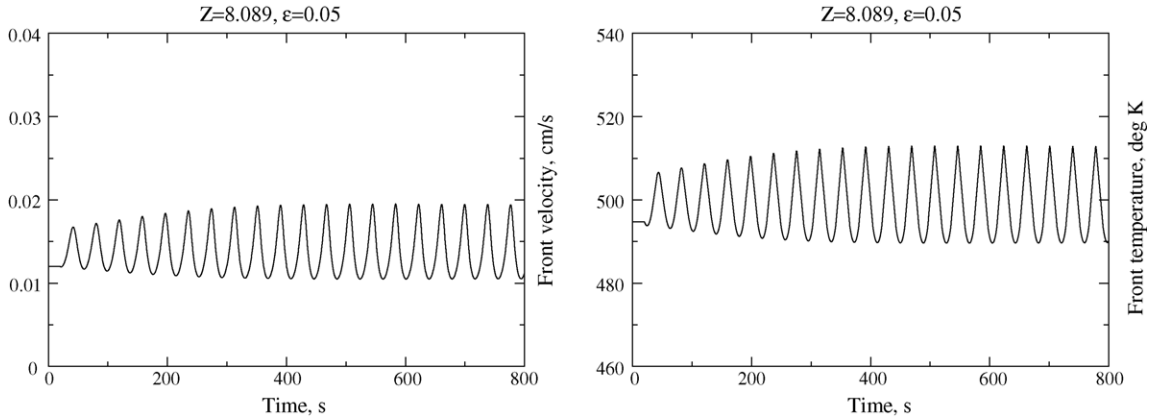

Fig. 8. Front velocity (left) and front temperature (right) profiles for the Arrhenius kinetics.

tonically decreases with time. If the computations are run for a longer time, the front pulsations die down, leading to the uniformly propagating polymerization front that will eventually disappear through the combination of the bulk and frontal polymerization discussed in the previous example.

The stabilization of the polymerization front becomes even more pronounced as Zeldovich number Z decreases toward the stability threshold (Fig. 10). The values of Z and ϵ in Fig. 10 correspond to $\alpha = 1.005$ and the criterion (17) indicates the stability of a uniformly propagating solution of (3) and (4). The system, however, is still clearly unstable with respect to front pulsations, as the initial stages of front propagation are characterized by the increased amplitude of pulsations even though the appropriate restriction of the traveling wave solution to (3) and (4) was used as the initial data. The same benchmark was used in [24] to distinguish between stable and unstable front dynamics. We attribute this apparent discrepancy to the approximate character of the criterion (17). Observe that the amplitude of front pulsations remains the same for the systems governed by the Arrhenius kinetics with the cutoff and step-function kinetics (Fig. 11), while pulsations essentially disappear in the system governed by the full Arrhenius kinetics. Hence, the instability criterion (17) used in [24] may fail on the long time scale.

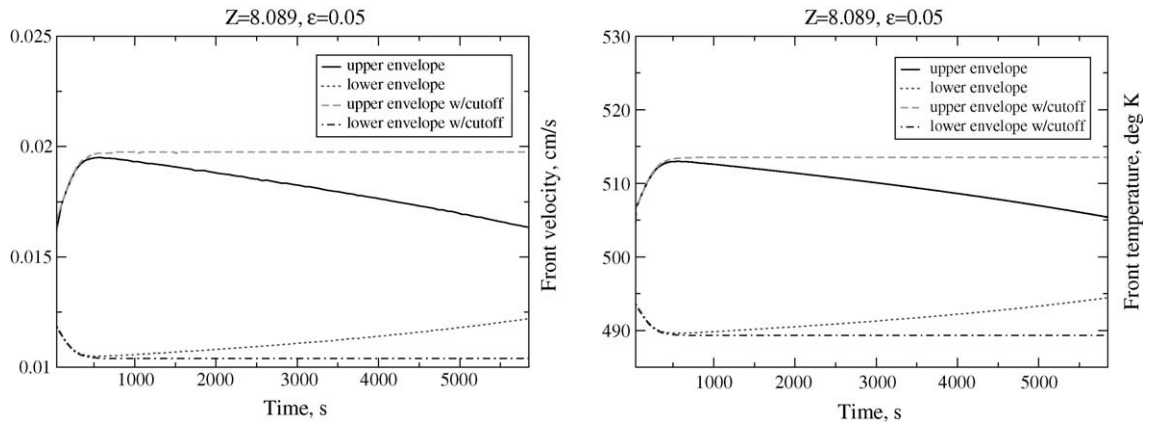

Fig. 9. Upper and lower envelopes of the front velocity (left) and the front temperature (right) profiles for the Arrhenius kinetics and the Arrhenius kinetics with cutoff.

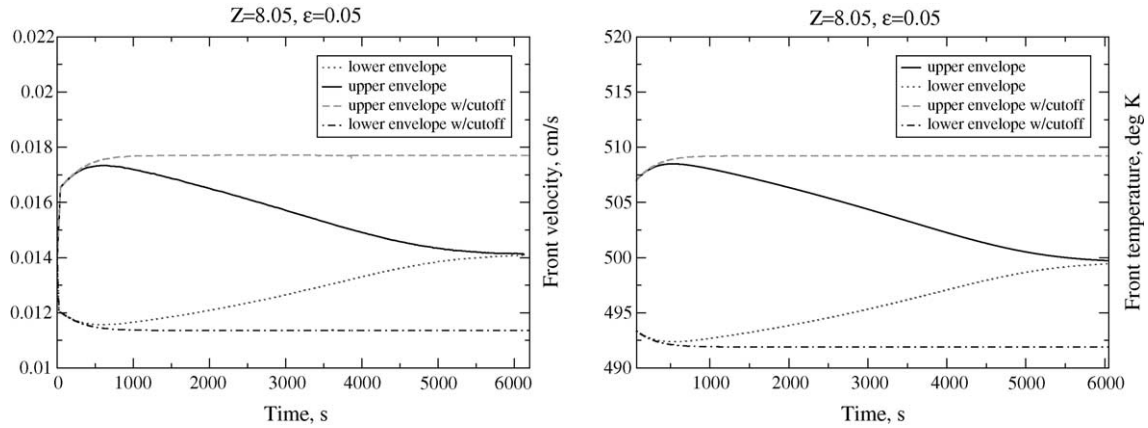

Fig. 10. Upper and lower envelopes of the front velocity (left) and the front temperature (right) profiles for the Arrhenius kinetics and the Arrhenius kinetics with cutoff.

Fig. 12 shows the evolution of Z_{eff} for systems with $Z = 8.05$ and $\epsilon = 0.05$. The effective Zeldovich number decreases in a system governed by the Arrhenius kinetics and remains constant in systems governed by discontinuous kinetics. We have also plotted in Fig. 12 the evolution of Z_{eff} for a system governed by the Arrhenius kinetics in the absence of heat diffusion. Note that the curve for Z_{eff} for this system coincides with the curve for the system with Arrhenius kinetics when the thermal diffusivity $\kappa \neq 0$ thus indicating that the time scale for heat diffusion is sufficiently long so that the heat from the frontal reaction does not affect the regions sufficiently far ahead of the reaction zone. The stabilizing phenomenon results from reactions in the bulk rather than from heat generated by the frontal reaction.

As another test of this hypothesis we use the following numerical experiment. We choose a large time $t = 4400$ s and consider a system governed by the Arrhenius kinetics *with a cutoff* (all bulk reactions ahead of the front have thus been switched off) with $M(x, 4400)$ and $T(x, 4400)$ as initial conditions.

The evolution of velocity envelopes for this system is presented in Fig. 13. The system governed by the Arrhenius kinetics with a cutoff and initial conditions $M(x, 0)$ and $T(x, 0)$ is characterized by velocity pulsation of constant amplitude (Fig. 11). On the other hand, velocity pulsations decay in the system governed by

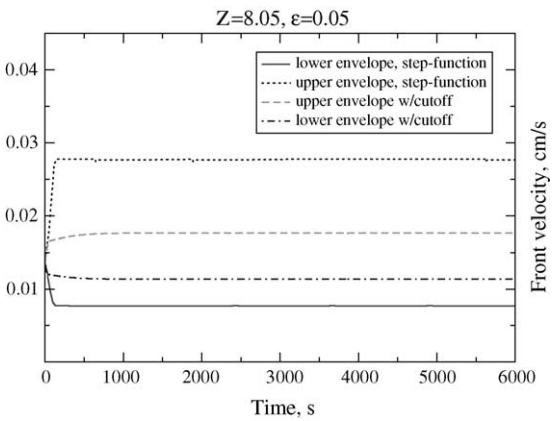

Fig. 11. Upper and lower envelopes of the front velocity for the Arrhenius kinetics with cutoff and step-function kinetics.

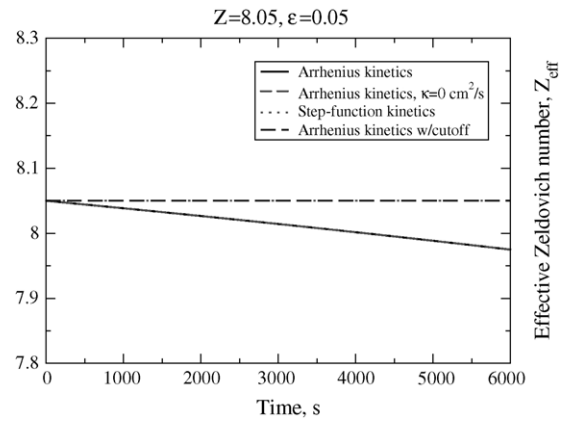

Fig. 12. Evolution of the effective Zeldovich number for various types of kinetics.

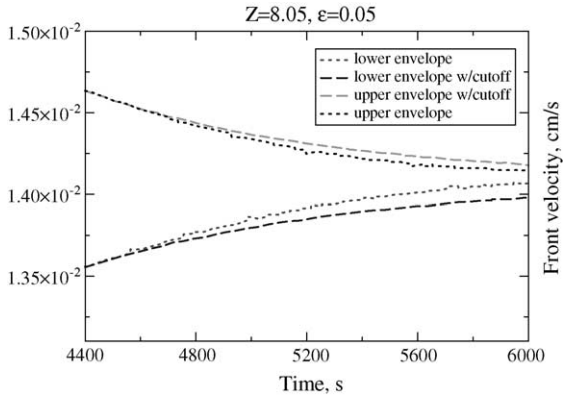

Fig. 13. Upper and lower envelopes of the front velocity for the Arrhenius kinetics with cutoff and step-function kinetics.

the Arrhenius kinetics with a cutoff when $M(x, 4400)$ and $T(x, 4400)$ are used as initial data. We conclude that Z_{eff} passes the stability threshold for the uniformly propagating reaction wave for some $t \in (0, 4400)$.

Observe that the amplitude of velocity oscillations decreases slightly faster for the system with Arrhenius kinetics than for the system with Arrhenius kinetics with a cutoff (Fig. 13) due to the presence of bulk reactions that suppress the effective Zeldovich number even further.

Note that the long time scale for our choice of parameters is on the order of 1 h, and the average front velocity is approximately 50 cm/h. The amount of time necessary for stabilization to become pronounced depends on the size of the test tube and parameters of the problem—the closer is the system to the stability threshold, the more significant the stabilization effect of the bulk reaction will become. For the values of parameters in Fig. 10 the decay in the amplitude of velocity/temperature oscillations becomes apparent in ≈20 min—the time comparable to the duration of a typical frontal polymerization experiment.

2.4. Solution features for distributed kinetics: frontal versus bulk effects

2.4.1. Pockets of unreacted monomer

The systems governed by various one-step kinetics discussed in this paper exhibit a similar hierarchy of intermediate-time solution dynamics that range from traveling wave propagation to a chaotic pulsation mode [14,10,24,12,17]. The dynamics mirror the sequence presented in Fig. 1 for the Arrhenius kinetics. In all cases the type of dynamics depends on values of nondimensional parameters of the problems—ϵ and the Zeldovich number Z. In the previous section we have demonstrated for the Arrhenius kinetics that the reaction cannot be considered to occur strictly in a frontal mode, as the bulk reactions are always present; the propagation, however, can be approximated as being frontal on intermediate time scales, since the bulk reactions are slow. Here we show that, in fact, polymerization can be considered to be purely frontal only for uniformly propagating reaction waves in systems governed by kinetics that ignore low-temperature bulk reactions. That is, for Zeldovich numbers beyond the first critical threshold (pulsating mode) there *always* exists a non-frontal component of the dynamics. In particular, we show that the monomer profile periodically becomes non-monotone in the regions experiencing high front acceleration, and pockets of unreacted monomer form behind the rapidly advancing front. These pockets later disappear via bulk polymerization.

We begin by considering systems governed by the full Arrhenius kinetics when the value of the Zeldovich number exceeds the traveling wave stability threshold. We set $Z = 10$ and $\epsilon = 0.05$; then the front propagates via a doubly-periodic pulsating mode (cf. Fig. 3).

In this regime, the polymerization front evolves by constantly cycling through the series of three distinct motions. First, the front slowly diffuses into the fresh mixture of reagents; this process is followed by a rapid "sharpening" of the front, which then quickly propagates while slowing down and widening at the same time (Fig. 14).

The interesting feature of this type of propagation is that its "sharpening" stage is very rapid and appears to occur in a bulk regime, since the monomer is depleted simultaneously everywhere within a wide reaction zone. Furthermore, the reaction rate remains higher in the front of the reaction zone leading to the appearance of a pocket of unreacted monomer at the tail of the front; the front subsequently detaches from the monomer pocket. The pocket persists for several seconds leaving it far behind the rapidly advancing polymerization front and then disappears via bulk polymerization.

The successive profiles of the monomer and temperature concentrations shown in Fig. 14 demonstrate the dynamics of the monomer pockets; the "zoomed-in"

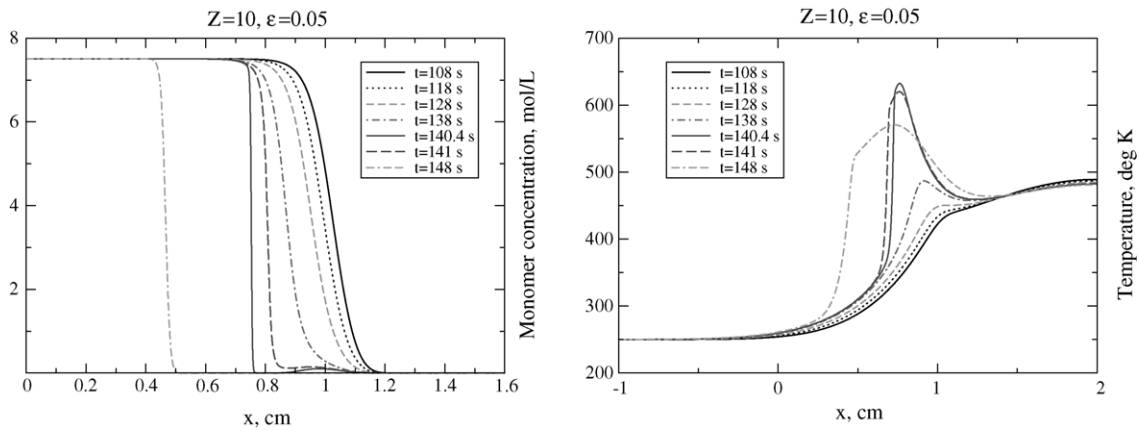

Fig. 14. Pockets of unreacted monomer behind the polymerization front: snapshots of monomer concentration and temperature profiles. The front advances to the left.

version of Fig. 14 is depicted in Fig. 15. The plots of both the position of the front (defined as in Section 2.1) and the position of the secondary maximum of the concentration profile shown in Fig. 16 illustrate the periodic nature of the effect. Note that for values of time for which two graphs in Fig. 16 coincide, the concentration profile is a monotone function of x and the secondary maximum does not exist.

In pulsating propagation, the appearances of monomer pockets and the temperature spikes in the mixture appear to be correlated (cf. Fig. 14). Note that the existence of pockets of reagents behind the combustion front was alluded to in [24], however, it is not clear whether the evidence of their existence was numerical or experimental.

Before trying to uncover the reasons for the existence of the monomer pockets, we want to rule out the possibility that they are simply numerical artifacts resulting e.g. from numerical under-sampling. We have already pointed out that our code exhibits very little numerical dissipation—this was indicated by Fig. 2 for the enthalpy H of the system defined by (8). Furthermore, although our algorithm is not adaptive, since the original problem was posed in one dimension, simple grid refinement throughout the domain is not too computationally expensive.

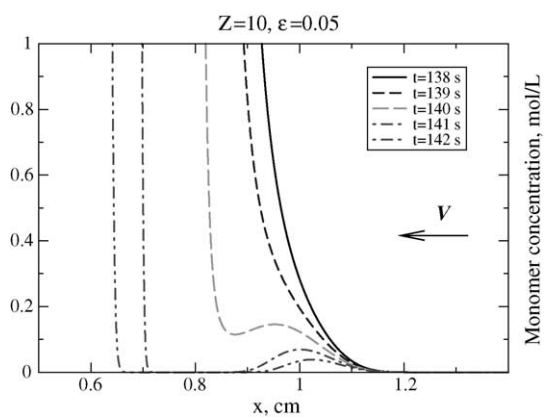

Fig. 15. Pockets of unreacted monomer behind the polymerization front: zoomed-in snapshots of the monomer concentration profile.

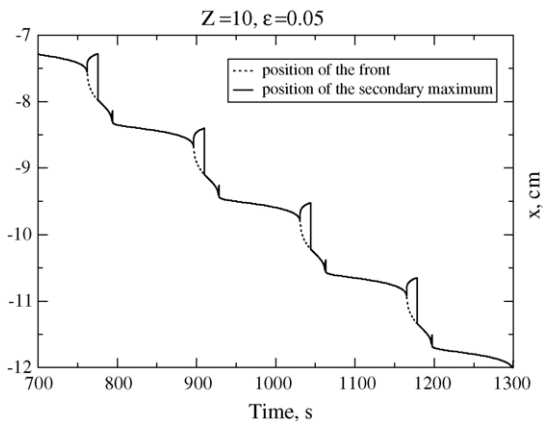

Fig. 16. Positions of the polymerization front and the secondary maximum of the concentration profile.

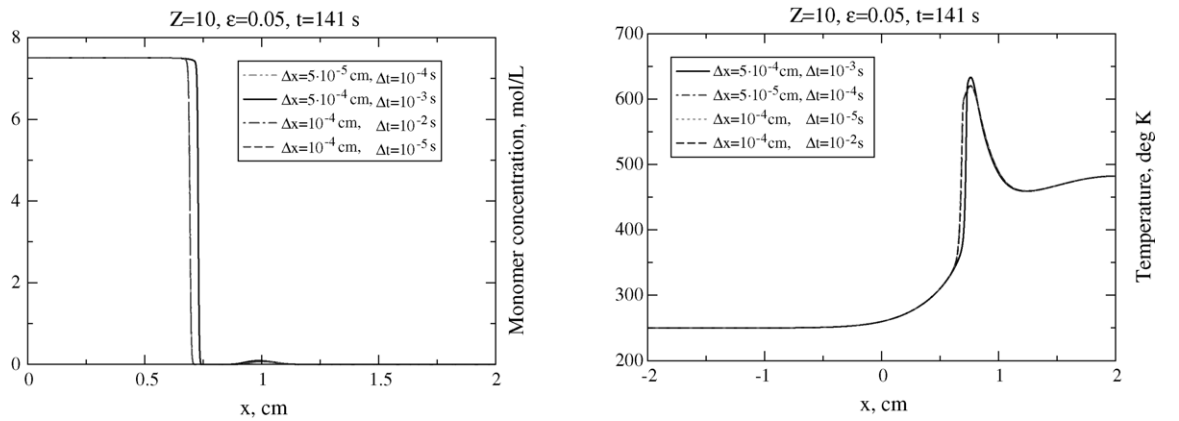

Fig. 17. Comparison of computed monomer concentration and temperature profiles for various time steps and grid sizes.

The calculations of temperature and monomer profiles are shown in Fig. 17 for various time steps and mesh sizes. Except for the case Δx =5.E−4, the results are indistinguishable—grid refinement clearly indicates numerical convergence and all sharp features are resolved and grid independent. In fact, the number of grid points in the regions of high gradients never falls below 100. Even when Δx = 5.E−4, the solution profiles are essentially the same, except for a small time shift. We conclude that non-monotone monomer distributions with the regions of non-zero monomer concentration behind a polymerization front correspond to a true solution of the governing system of equations.

2.4.2. *Rationale for the existence of pockets of unreacted monomer*

We begin this section by considering the following numerical experiment. As is shown in Fig. 14 the monomer concentration profile at $t = 138$ s is monotone. Consider the monomer concentration and the temperature profiles when $t = 138$ s as initial conditions for a polymerization system in which the heat diffusion is negligible ($\kappa = 0$). Then the governing system of Eqs. (3)–(5) reduces to a coupled system of ODEs with the spatial coordinate x as parameter. This system can be solved either by setting $\kappa = 0$ in our code or by using Maple. The solution profile for $t = 140.4$ s obtained with our code when $\kappa = 0$ is presented in Fig. 18.

The monomer profiles for systems with and without diffusion in Fig. 18 appear to be qualitatively similar, especially when $x > 0.95$ where the influence of heat diffusion is, therefore, the weakest. Further, the monomer and the temperature distributions at $t = 138$ s appear to be such that, in the absence of heat diffusion, the regions with higher monomer concentration experience complete conversion faster than the regions with lower monomer concentration. Although this might appear as an indication of a higher temperature in monomer-rich regions of the gradient zone when $t = 138$ s, we will soon see that it is not necessarily so.

Consider again the system of ODEs describing the evolution of temperature and monomer concentrations in the system without heat diffusion with $M(x, t)$ and $T(x, t)$ as the initial data. Then Eqs. (3)–(5) take the

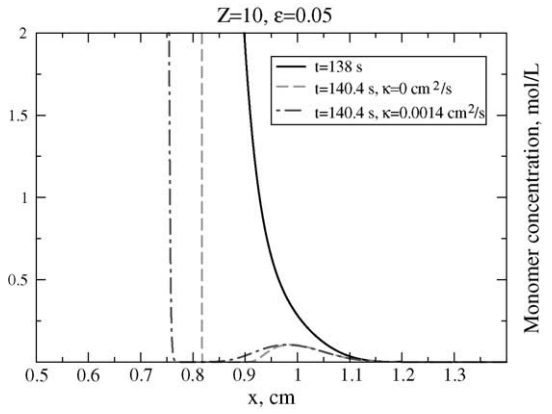

Fig. 18. Comparison of monomer concentrations in systems with and without heat diffusion.

form

$$\begin{cases} \dfrac{\partial \tilde{M}}{\partial \tilde{t}} = -k\tilde{M}\mathrm{e}^{E/R_g T_b(1-(T_b/\tilde{T}))}, & \tilde{t} > t, \\ \dfrac{\partial \tilde{T}}{\partial \tilde{t}} = kq\tilde{M}\mathrm{e}^{E/R_g T_b(1-(T_b/\tilde{T}))}, & \tilde{t} > t, \\ \tilde{M}(x,t) = M(x,t),\ \tilde{T}(x,t) = T(x,t). \end{cases} \tag{23}$$

Since the enthalpy density $\tilde{h}(x,\tilde{t}) = q\tilde{M}(x,\tilde{t}) + \tilde{T}(x,\tilde{t})$ is conserved

$$\tilde{h}(x,\tilde{t}) = qM(x,t) + T(x,t) = h(x,t),$$

pointwise in x, we can express $\tilde{T}$ in terms of $\tilde{M}$ and reduce the system (23) to a single ODE that can be solved to obtain an implicit equation

$$\tilde{t} = k^{-1}\mathrm{e}^{-1/\epsilon}\left[\mathrm{Ei}\left\{\frac{T_b}{\epsilon(h(x,t)-q\tilde{M}(x,\tilde{t}))}\right\} - \mathrm{Ei}\left\{\frac{T_b}{\epsilon T(x,t)}\right\}\right] + k^{-1}\mathrm{e}^{(T_b-h(x,t))/\epsilon h(x,t)}\left[\mathrm{Ei}\left\{\frac{qT_b M(x,t)}{\epsilon h(x,t)T(x,t)}\right\} - \mathrm{Ei}\left\{\frac{qT_b\tilde{M}(x,\tilde{t})}{\epsilon h(x,t)(h(x,t)-q\tilde{M}(x,\tilde{t}))}\right\}\right] \tag{24}$$

for $\tilde{M}(x,\tilde{t})$ where $\mathrm{Ei}(\cdot)$ is the exponential integral. Viewed differently, given the initial data $T(x,t)$ and $M(x,t)$ at the time t, the Eq. (24) determines the time necessary to reach the prescribed monomer concentration $\tilde{M}$ at the point x in the absence of heat diffusion. Since the monomer concentration in our mathematical model never vanishes, we will postulate that the conversion process at the point x is complete when the monomer concentration at x falls below some small prescribed value m to be chosen later (cf. Section 2.1). Substituting m for $\tilde{M}$ into (24) we obtain a *conversion time* function

$$\tilde{t}(x,t) := k^{-1}\mathrm{e}^{-1/\epsilon}\left[\mathrm{Ei}\left\{\frac{T_b}{\epsilon(h(x,t)-qm)}\right\} - \mathrm{Ei}\left\{\frac{T_b}{\epsilon T(x,t)}\right\}\right] + k^{-1}\mathrm{e}^{(T_b-h(x,t))/\epsilon h(x,t)}\left[\mathrm{Ei}\left\{\frac{qT_b M(x,t)}{\epsilon h(x,t)T(x,t)}\right\} - \mathrm{Ei}\left\{\frac{qT_b m}{\epsilon h(x,t)(h(x,t)-qm)}\right\}\right]. \tag{25}$$

We will use the function $\tilde{t}(x,t)$ to estimate the conversion time in systems where the heat diffusion is small but not negligible.

Consider again the polymerization process when $Z = 10$ and $\epsilon = 0.05$ and suppose that m=1.E−3—for given values of Z and ϵ this threshold is sufficient to resolve the fine monomer profile features. In Fig. 19 we present the temperature, monomer concentrations, and conversion time profiles at three different times. When $t = 125$ s, the "wide" polymerization front slowly "diffuses" into the unreacted monomer. When $t = 141$ s the front is at the final stages of the front sharpening process, and when $t = 157$ s, the front is in the fast propagation regime.

As indicated by dimensionless PDEs (12) and (13), for small ϵ and $T < 1$ (dimensional $T < T_b$), the reaction slows down with an increasing Z when T is away from 1. On the other hand, the reaction accelerates when T is sufficiently close to 1. If initially the front is very sharp and the temperature in the reaction zone is not too high, then for large Z we expect that the monomer concentration should decrease slowly in the zone adjacent to the front containing the fresh monomer. Hence, the front widens via its slow diffusion into the monomer. This process is accompanied by the slow rise in the temperature in the same region. This results in the monomer concentration and temperature profiles depicted in Fig. 19 for $t = 125$ s.

Note that for $t = 125$ in Fig. 19, the temperature at the point of the minimum conversion time is lower than the temperature at the point of the maximum conversion time. The concentration of unreacted monomer near the point of minimum conversion time is higher than the concentration near the point of the local maximum conversion time. This can be explained by the fact that although the initial temperature/reaction rate can be lower for a point with higher monomer concentration, the amount of heat released during the reaction is higher for the regions with higher monomer concentration leading to faster conversion times.

The combination of reaction and heat diffusion in the direction of the unreacted monomer zone raises the temperature of the reagent in the part of the reaction zone where the concentration of the monomer is close to its initial value. In the absence of heat diffusion,

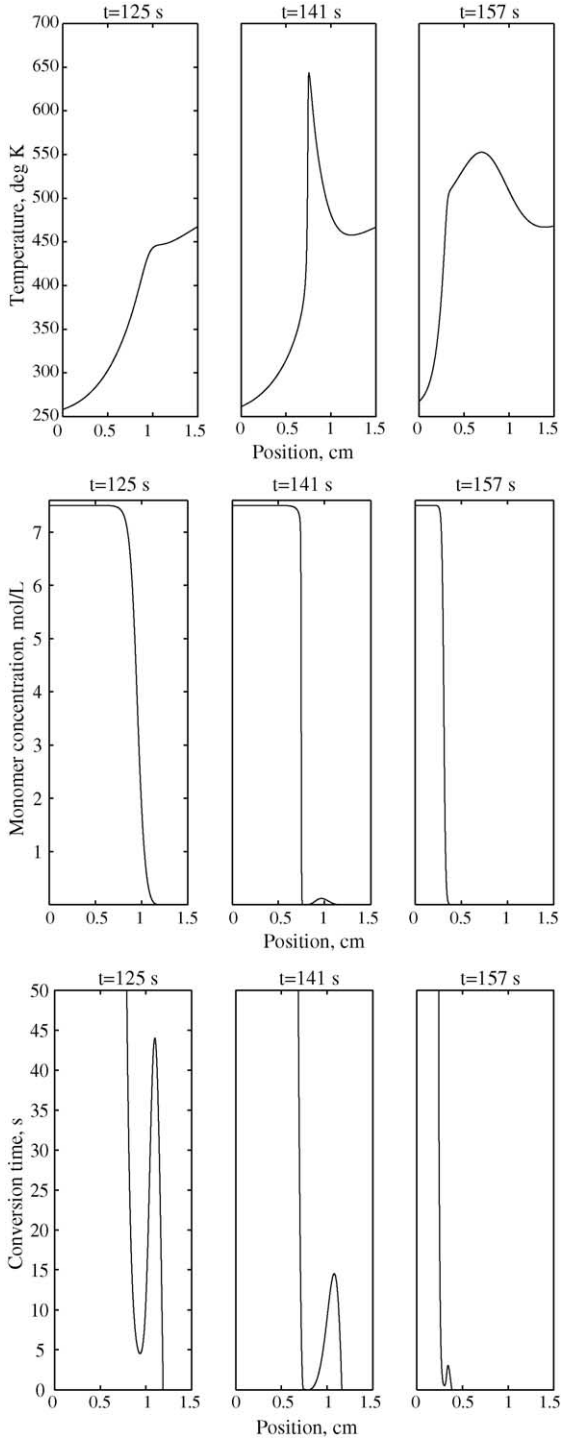

Fig. 19. Temperature, monomer concentrations, and conversion time profiles in a system with $Z = 10$ and $\epsilon = 0.05$.

the resulting large difference in the local maximum and minimum conversion times for $t = 125$ s sets the stage for the formation of a monomer pocket at about $t = 130$ s.

Near the point of the minimum conversion time for $t = 125$ s, the reaction rate is high by definition. Correspondingly, the heat release begins to dominate the heat diffusion. Further, the heat flux toward the cooler, unreacted monomer exceeds the flux toward the products of the reaction. We conclude the plot of conversion time for $t = 125$ s should qualitatively predict the structure of the solution for $t > 125$ s, as is confirmed by the monomer profile for $t = 141$ s in Fig. 19.

Fig. 19 shows that the reaction immediately to the right of $x = 1$ appears to proceed at about the same constant temperature at $t = 141$ s as at $t = 125$ s suggesting lack of substantial heat diffusion. Hence, the conversion time as predicted by (24) should be fairly accurate. Fig. 18 confirms the appropriateness of using the adiabatic model near $x = 1$. The actual conversion time for the monomer pocket should be somewhat lower due to the heat diffusion.

The above discussion implies that the monomer-to-polymer transition between $t = 125$ s and $t = 141$ s occurs essentially via the bulk mode; beyond $t = 141$ s it is via the combination of the bulk and the frontal mode until the monomer pocket disappears completely at some time before $t = 157$ s. The evolution then proceeds purely in the frontal mode until the sharp front

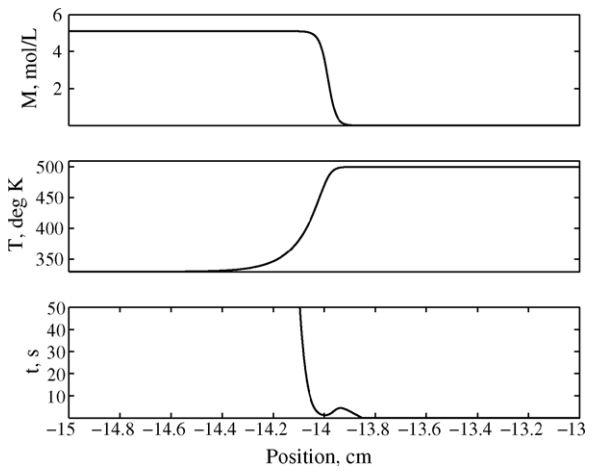

Fig. 20. Temperature, monomer concentrations, and conversion time profiles in a system with $Z = 7$ and $\epsilon = 0.05$.

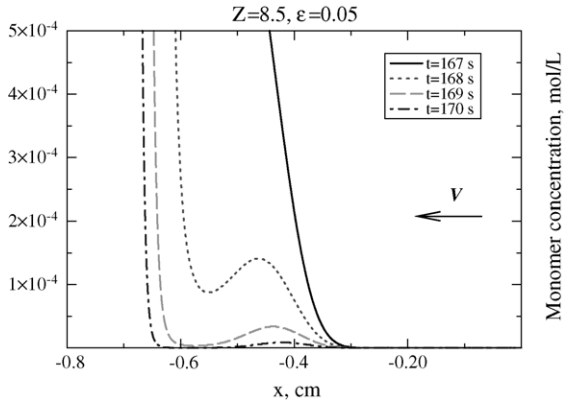

Fig. 21. Pockets of unreacted monomer behind the polymerization front propagating via a periodic pulsating mode in a system governed by Arrhenius kinetics: zoomed-in snapshots of the monomer concentration profile.

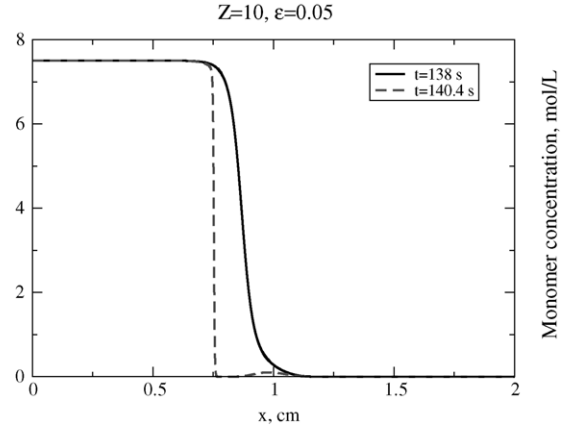

Fig. 22. Pockets of unreacted monomer behind the polymerization front propagating via a periodic pulsating mode in a system governed by Arrhenius kinetics with a cutoff.

quickly reaches the regions with lower temperature and slows down. The propagation mechanism then repeatedly cycles through the same modes as outlined above.

Because of the presence of heat diffusion, the small dip in the conversion time for $t = 157$ s in Fig. 19 does not lead to the formation of a monomer pocket. The adiabatic model predicts the differences in conversion time between the head and the tail of the front. However, the heat diffusion levels off these differences. Indeed, the same effect is indicated for the system with traveling-wave-type front ($Z = 7$) as evidenced by Fig. 20.

An important observation that follows from the above discussion is that the polymerization process in a doubly-periodic pulsating propagation, e.g. $Z = 10$, $\epsilon = 0.05$ considered throughout this section, *cannot* be described by using a point-source kinetics such as in [14]. Features like monomer pockets will never appear since all bulk reactions are neglected.

Next we will examine whether non-monotonicity of monomer concentration profile is characteristic of other types of pulsating propagation for Arrhenius and other types of distributed kinetics.

First, consider a polymerization system governed by Arrhenius kinetics when $Z = 8.5$ and $\epsilon = 0.05$. On an

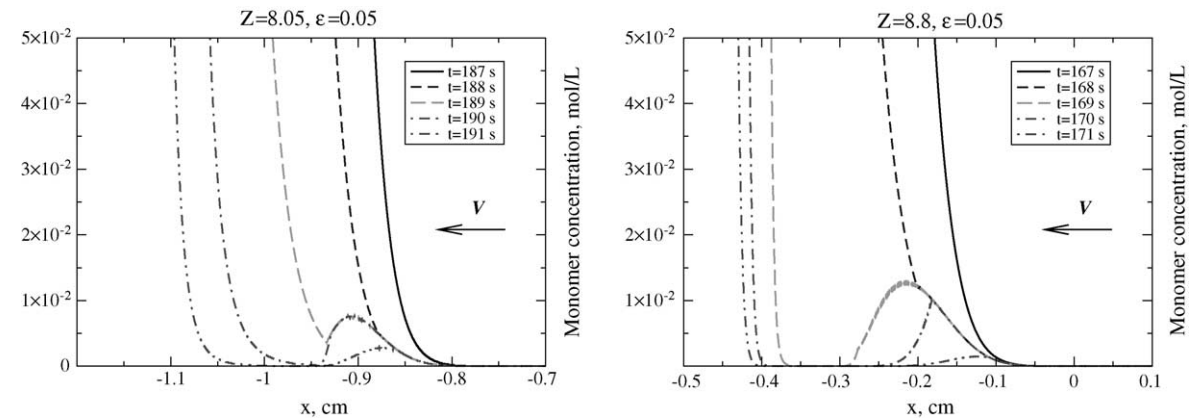

Fig. 23. Pockets of unreacted monomer behind a periodic and doubly periodic pulsating polymerization front in a system governed by step-function kinetics.

intermediate time scale, a polymerization front in this system propagates in a periodic pulsating mode. The monomer pocket formation can still be clearly observed in this case (Fig. 21); the concentration of monomer in the pocket is, however, several orders of magnitude lower than the concentration in similar pockets in doubly-periodic propagation (Fig. 15). We conjecture that the maximum concentration of monomer within a pocket rises with an increase in Zeldovich number.

When a polymerization system with $Z = 10$ and $\epsilon = 0.05$ is governed by the Arrhenius kinetics with a cutoff (18), the monomer dynamics at an intermediate time scale is essentially the same as for the Arrhenius kinetics (Fig. 22). The formation of monomer pockets behind a polymerization front can also be observed in systems governed by the step-function kinetics, both in a periodic pulsations and in a doubly-periodic pulsations mode (Fig. 23). Note that non-smoothness of monomer concentration profiles in Fig. 23 is due to the discontinuous character of step-kinetics.

In summary, we demonstrated that all distributed kinetics studied in this paper that are known to exhibit the hierarchy of modes of front propagation—traveling wave, periodic pulsating, doubly-periodic pulsating, etc.—cannot be fully described in terms of frontal polymerization alone beyond the steady traveling wave regime. The bulk mode of monomer conversion becomes important when a wide front evolves to a sharp front resulting in a formation of a monomer pocket that subsequently disappears via a bulk polymerization. These effects cannot be captured in point-source kinetics where the bulk reaction is ignored.

Further, note that for pulsating fronts the assumption that the width of the reaction zone is of order ϵ is generally invalid (Fig. 14).

We conclude this section by plotting the monomer concentration, temperature, and the conversion time when $Z = 10$ and $\epsilon = 0.05$ as functions of both time and spatial coordinate (Fig. 24). The two-dimensional figures presented throughout this section correspond to sections of these plots by planes perpendicular to the time-axis. Note that the perspective for the temperature is different than that for two other plots.

The monomer pockets in Fig. 24 are represented by small protrusions in the concentration plot pointing in the direction of time-axis. The monomer pockets survive for sufficiently long time to exist well behind the front—the right-most pocket centered near $x = 1.1$ cm disappears around $t = 175$ s when the front is located at about $x = 0.5$ cm. The related local maxima of conversion time and the temperature spikes can be clearly seen on the respective plots.

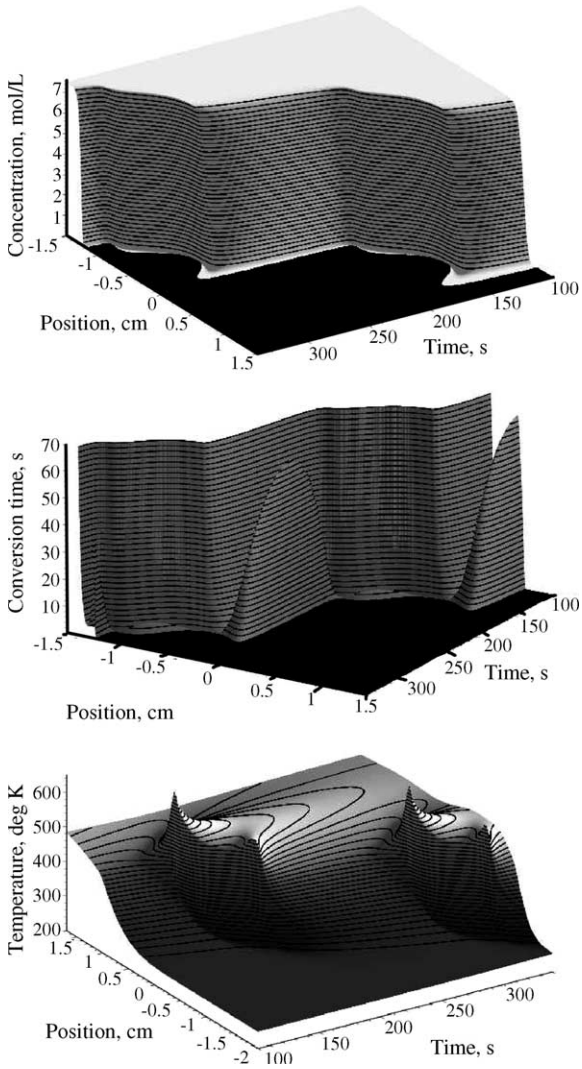

Fig. 24. Monomer concentration, conversion time, and temperature as functions of x and t.

3. Conclusions

We considered a one-step kinetics model of free-radical frontal polymerization in which a monomer-

initiator mixture is converted into a polymer via a propagating self-sustaining reaction front. We demonstrated that some of the assumptions that are valid in combustion problems may lead to incorrect results in FP, mainly because of the differences in the magnitudes of non-dimensional parameters in frontal polymerization versus gasless combustion.

We showed that the long-time behavior of systems modeled with step-function and cutoff kinetics significantly departs from the long-time behavior of systems modeled with Arrhenius kinetics mainly due to the influence on front dynamics of slow bulk reactions in the initial mixture of reagents. These reactions can be neglected in combustion problems because of very high speeds of front propagation; however they may play a role in FP where these speeds are much slower.

Further, for all types of distributed kinetics considered in this paper, we demonstrated the existence of pockets of unreacted monomer behind pulsating polymerization fronts. The time evolution of these pockets proceeds via bulk polymerization. Hence, the "true" frontal polymerization in systems governed by distributed kinetics is possible only when bulk reactions ahead of the front are neglected and only for fronts that propagate with a constant speed.

Although the systems governed by the full Arrhenius kinetics and its point-source approximations generally exhibit the same spectrum of solution behavior, the stability thresholds for uniformly propagating fronts generally differ for different kinetics. The discrepancy may be attributed to the effect of the bulk reaction that is usually neglected for point-source-type kinetics. The monomer and temperature profiles in systems governed by the distributed kinetics have features that cannot be described by point-source-type kinetics. In our numerical experiments we observed that the relative magnitude of these features appears to increase as Zeldovich number increases. It will be of interest to examine whether the rise of these features signifies the widening discrepancy between the dynamics of solutions for distributed and point-source kinetics. Stated differently, since the point-source kinetics is not usually obtained from the full Arrhenius kinetics via a rigorous asymptotic procedure, how accurate is the point-source kinetics approximation for the values of the Zeldovich number beyond the stability threshold for the uniformly propagating reaction waves?

We have also shown that the assumption that the width of the reaction zone is of order ϵ is generally invalid for pulsating fronts.

Acknowledgements

The authors would like to express their gratitude to V.A. Volpert for the valuable discussions and to the referees for the comments on the draft of this manuscript.

References

[1] K.M. Chechilo, R.Y.A. Khvilivitskii, N.S. Enikolopyan, Phenomenon of polymerization reaction spreading, Doklady Akademii Nauk. SSSR 205 (1972) 1180–1181.
[2] Y. Chekanov, D. Arrington, G. Brust, J.A. Pojman, Frontal curing of epoxy resins: comparison of mechanical and thermal properties to batch-cured materials, J. Appl. Polym. Sci. 66 (1997) 1209–1216.
[3] M.F. Perry, V.A. Volpert, L.L. Lewis, H.A. Nichols, J.A. Pojman, Free-radical frontal copolymerization: the dependence of the front velocity on the monomer feed composition and reactivity ratios, Macromolec. Theory Simulat. 12 (2003) 276–286.
[4] Y. Choi, J.K. Lee, M.E. Mullins, Densification process of TiC_x-nicomposites formed by self-propagating high-temperature synthesis reaction, J. Mater. Sci. 32 (1997) 1717–1724.
[5] A.G. Merzhanov, A.K. Filonenko, I.P. Borovinskaya, New phenomena in combustion of condensed systems, Doklady Akademii Nauk. SSSR 208 (1973) 122–125.
[6] A.G. Merzhanov, B.I. Khaikin, Theory of combustion waves in homogeneous media, Proc. Energy Combust. Sci. 14 (1988) 1–98.
[7] A.B. Sawaoka, Shock Waves in Materials Science, Springer-Verlag, Tokyo, 1993.
[8] A.M. Khan, J.A. Pojman, The use of frontal polymerization in polymer synthesis, Trends Polym. Sci. 4 (1996) 253–257.
[9] W.A. Sirignano, A.G. Merzhanov, L.D. Luca (Eds.), Advances in Combustion Science: In Honor of Ya. B. Zel'dovich, American Institute of Aeronautics and Astronautices, Inc., USA, 1997.
[10] S.E. Solovyov, V.M. Ilyashenko, J.A. Pojman, Numerical modeling of self-propagating polymerization fronts: the role of kinetics on front stability, Chaos 7 (1997) 331–340.
[11] C.A. Spade, V.A. Volpert, On the steady-state approximation in thermal free radical frontal polymerization, Chem. Eng. Sci. 55 (2000) 641–654.
[12] D.A. Schult, V.A. Volpert, Linear stability analysis of thermal free radical polymerization waves, Int. J. Self-Propagat. High-Temp. Synth. 8 (1999) 417–440.
[13] D.A. Schult, Matched asymptotic expansions and the closure problem for combustion waves, SIAM J. Appl. Math. 60 (1) (1999) 136–155.

[14] B.J. Matkowsky, G. Sivashinsky, Propagation of a pulsating front in solid fuel combustion, SIAM J. Appl. Math. 35 (1978) 465–477.
[15] G. Sivashinsky, Structure of Bunsen flames, J. Chem. Phys. 62 (1975) 638–643.
[16] A.P. Aldushin, S.G. Kasparyan, Thermodiffusional instability of a stationary flame wave, Tech. rep., Institute of Chemical Physics, Chernogolovka, preprint, 1978.
[17] D. Golovaty, On step-function kinetics of frontal polymerization, SIAM J. Appl. Mater., submitted for publication.
[18] A. Bayliss, B.J. Matkowsky, Fronts, relaxation oscillations, and period doubling in solid fuel combustion, J. Comput. Phys. 71 (1987) 147–168.
[19] A.P. Aldushin, S.G. Kasparyan, Thermodiffusional instability of a combustion front, Sov. Phys. Dokl. 24 (1979) 29–31.
[20] L.K. Gross, V.A. Volpert, Weakly nonlinear stability analysis of frontal polymerization, Stud. Appl. Math. 110 (2003) 351–375.
[21] A. Bayliss, B.J. Matkowsky, Two routes to chaos in solid fuel combustion, SIAM J. Appl. Math. 50 (1990) 437–459.
[22] I. Brailovsky, G. Sivashinsky, Chaotic dynamics in solid fuel combustion, Physica D 65 (1993) 191–198.
[23] M. Frankel, V. Roytburd, G. Sivashinsky, Complex dynamics generated by a sharp interface model of self-propagating high-temperature synthesis, Combust. Theory Model. 2 (1998) 1–18.
[24] K.G. Shkadinskii, B.I. Khaikin, A.G. Merzhanov, Propagation of a pulsating exothermic reaction front in the condensed phase, Fizika Goreniya i Vzryva 1 (1971) 19–28 (English translation in Combust. Expl. Shock Waves 7 (1971) 15–22).
[25] P. Dimitriou, J. Puszynski, V. Hlavacek, On the dynamics of equations describing gasless combustion in condensed systems, Combust. Sci. Tech. 68 (1989) 101–111.
[26] Y.B. Zeldovich, A.P. Aldushin, S.I. Khudyayev, Numerical study of flame propagation in a mixture reacting at the initial temperature, Fizika gorenija i vzryva 15 (1979) 20–27.